Derivatives of Coenzyme F 430 with a Covalently Attached α-Axial Ligand

Part I

Evaluation of Suitable Spacer–Ligand Constructs by Molecular Modeling, Their Synthesis, and NMR Solution Structure

by **Carsten Bauer**[1]) and **Bernhard Jaun***

Laboratorium für Organische Chemie, ETH-Hönggerberg HCI CH-8093 Zürich

Dedicated to Professor *Duilio Arigoni* on the occasion of his 75th birthday

X-Ray structures of the enzyme methyl-coenzyme M reductase show that the Ni-center in the prosthetic group coenzyme F 430 is penta- or hexacoordinated with the carboxamide group of a glutamine residue occupying the axial coordination site on the α-side of the macrocycle. To obtain diastereoselectively coordinated complexes for mechanistic and spectroscopic studies of the free coenzyme in solution, we aimed to prepare partial-synthetic derivatives of coenzyme F 430 that have a coordinating group attached *via* a linker to one of the propanoic acid side chains. By using molecular-mechanics calculations and two different conformational search methods, a set of 50 structures containing imidazole or pyridine units as potential ligands were computationally tested according to geometric criteria defining coordinating conformations. The best candidates proved to be proline-containing tri- and tetrapeptides with a methyl-histidine as the C-terminal residue. These linkers were synthesized, and their conformation was determined by NMR. Refinement of the molecular modeling by using the experimentally determined geometric restraints allowed us to decide that the tripeptide Pro-Pro-His(π-Me)-OMe (**10**) was the most promising of all tested structures for attachment to the side chain at C(3) or C(13) of F 430.

Introduction. – Methyl-coenzyme M reductase (MCR) is the key enzyme in biological methane formation by *Archaea* [1][2]. It catalyzes the conversion of methyl-coenzyme M and coenzyme B to methane and the mixed disulfide of coenzymes M and B according to a still largely unknown mechanism [3][4] (see *Scheme 1*). The 300 kDa apoprotein consists of three different chains in a heterodimeric $\alpha_2\beta_2\gamma_2$ arrangement. Well resolved X-ray structures of inactive forms of MCR show two symmetry-related active sites, each containing one molecule of the hydrocorphinoid Ni-complex coenzyme F 430 (**1**) [5–8] tightly but not covalently bound to four of the six protein chains [9][10].

The axial coordination site on the β-face of the macrocycle[2]) is accessible to substrates and is occupied by different ligands in the MCR_{silent} and $MCR_{ox\text{-}silent}$ enzyme states for which high-resolution crystal structures are available [9]. In the α-axial position, however, the O-atom of a glutamine (Gln $\alpha/\alpha'147$) carboxamide group is found 2.3 Å from the Ni-ion in all crystal structures reported so far (*Fig. 1*).

---

[1]) Present address: The Burnham Institute, La Jolla Cancer Research Center, 10901 North Torrey Pines Road, La Jolla, 92037 CA, USA (e-mail: caba@burnham.org).

[2]) Rings A-B-C-D (in this order) are seen counterclockwise from the α-face, clockwise from the β-face.

Scheme 1

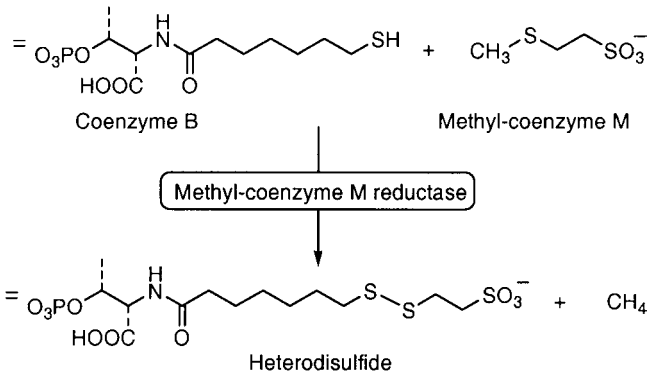

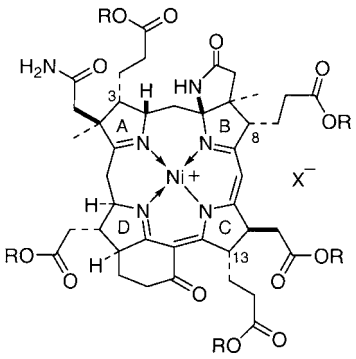

1 Coenzyme F430; R=H
2 Ni^{II} F430M; R=Me, $X=ClO_4$

The catalytically inactive, EPR-silent forms of MCR that have been crystallized contain coenzyme F 430M with the Ni-center in the Ni^{II} valence state. Other enzyme forms, in particular the active-state MCR_{red1}, have been shown to contain Ni^{I} F 430 [11–13], whereas the formal oxidation state of another inactive but EPR-visible form, MCR_{ox1}, is still disputed (Ni^{I} *vs.* Ni^{III}) [14–17]. The different mechanisms that have been proposed for catalysis by MCR have in common that they all postulate cycling among different oxidation states of the Ni-center during turnover [10][18–20]. Mechanistic and spectroscopic studies of free coenzyme F 430 (**1**) and its pentamethyl ester **2** (F 430M) in solution have been essential for our understanding of the redox and coordination chemistry of this hydrocorphinoid Ni-complex and form the basis of assigning oxidation states to the different enzyme forms by comparison of EPR/ENDOR [11–13][21–23], UV/VIS [12][13][21], EXAFS/XAS [24], and MCD spectra.

However, the approach to use the free coenzyme and its derivatives as models for the enzyme-bound forms reaches its limits whenever the role of ligands in the axial

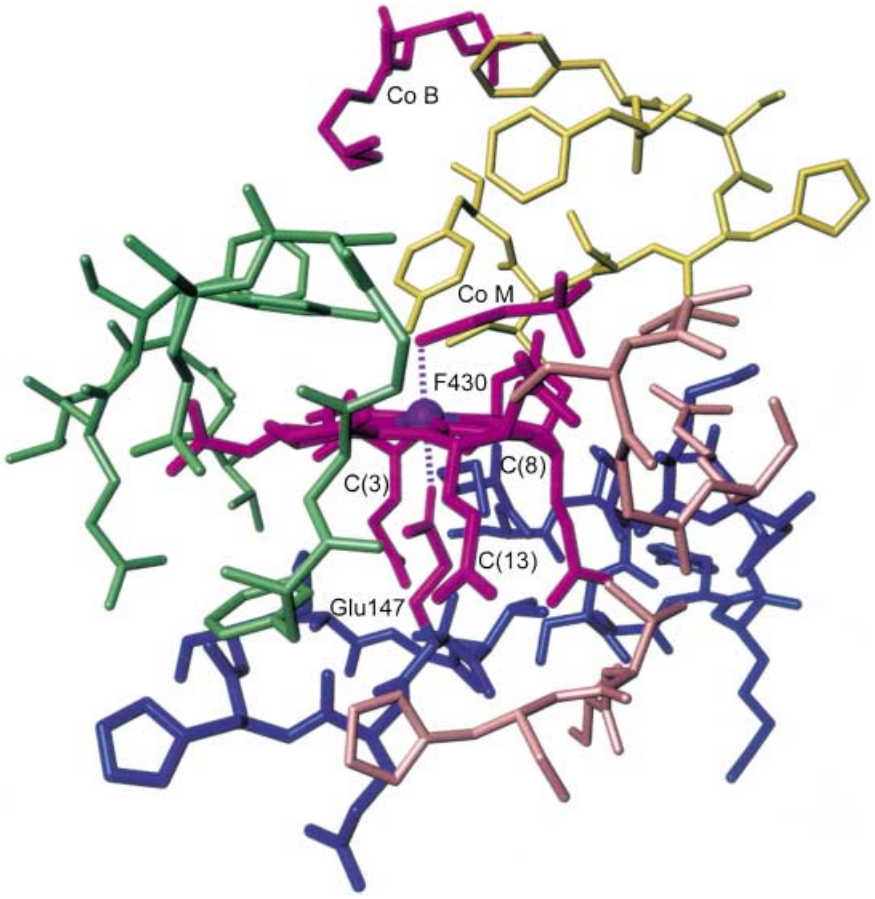

Fig. 1. *View of the active site of methyl-coenzyme M reductase in the* $MCR_{ox\text{-}silent}$ *state* (PDB ID 1MRO) [9]. Coenzyme F 430, coenzyme M, coenzyme B, and the glutamine side chain occupying the α-axial coordination site (Glu $^{\alpha 147}$) are shown in purple, the backbones of the four protein chains in blue, pink, green, and yellow (residues >10 Å from the Ni-center omitted).

positions is important. Because of the fast ligand exchange at labile Ni^{II} or Ni^{I}, it is impossible to generate pure diastereoisomers of pentacoordinated forms or mixed hexacoordinated complexes of free coenzyme F 430 in solution. As shown by the X-ray structures, axial ligands are present in all known Ni^{II} forms of the enzyme [1], and recent EPR/ENDOR studies have demonstrated interactions of the Ni^{I} center with the thiol(ate) S-atom of coenzyme M in the MCR_{red2} state [25]. To assess the influence of these ligands on the reactivity of F 430 and to obtain more-realistic models of the active site for solution studies it was, therefore, necessary to find ways to generate F 430 complexes with well-defined axial ligands. Here we report our project to make derivatives of coenzyme F 430 with a single α-axial ligand by covalently connecting the ligand to one of the propanoic acid side chains *via* a spacer. In *Part I* of this series, we describe the evaluation of suitable spacer–ligand structures by molecular modeling,

their synthesis, and their preferred conformations in solution as determined by NMR. In *Part II* [26a], we report the preparation and characterization of the five possible F 430 tetramethyl esters, the synthesis of a derivative in which the 3-propanoic acid side chain is linked to the selected spacer–ligand structure, and experimental proof that it does form an intramolecular pentacoordinated complex.

Evaluation of Potential Spacer–Ligand Combinations by Molecular Modeling. – Our search for optimal spacer–ligand structures was guided by the following considerations:

1) Because no crystal structures of isolated Ni^{II} F 430 are available, the X-ray structure of the $MCR_{ox\text{-}silent}$ form of the enzyme, which contains high-spin six-coordinate Ni^{II} F 430, had to serve as the structure template for the hydrocorphin macrocycle. This introduced a considerable degree of uncertainty, because it is not known how far the solution conformation of high-spin coenzyme F 430 deviates from the conformation in the enzyme.
2) In the enzyme, the carboxamide group of Gln^{147} occupies the α-axial coordination site. In solution, however, amides seem to be very weak ligands for Ni^{II} F 430 because, when primary amides were added in large excess to the pentamethyl ester **2** in nonpolar solvents, we did not observe the low-spin → high-spin transition typically induced by the addition of the first axial ligand [26b]. Since, at least for the first stage of the project, it was crucial to be able to establish that intramolecular coordination does indeed occur, we chose to use groups derived from pyridine and 1*H*-imidazole, which are known to form five- and six-coordinate complexes with Ni^{II} F 430M in solution, as potential ligands to be linked to the end of the spacer.
3) To obtain efficient intramolecular complexation, the free spacer–ligand molecule should ideally prefer a conformation that is preorganized for complexation when linked to one of the propanoic acid side chains of F 430. This translates into the geometric constraints depicted in *Fig. 2*, namely an U-shaped loop with a distance of *ca.* 6 Å between the coordinating N-atom and the heteroatom attached to the F 430 side chain, as well as an angle of *ca.* 120° between the axis of the lone pair forming a coordinative bond to the Ni-atom and the vector connecting the two ends of the loop.

A set of *ca.* 50 spacer–ligand combinations that appeared to be promising candidates upon inspection of molecular models were subjected to a conformational search by molecular-mechanics calculations. Among them were *meta*- and *para*-alkyl-substituted pyridine derivatives **3**–**9**, 8-alkylisoquinoline derivatives (structures not shown) and peptidic linkers like **10** and **11**. Each spacer-ligand structure was connected *in silico* to the 3- or 13-propanoic acid side chains of coenzyme F 430 (**1**) *via* a *trans*-amide or ester bond to generate the starting structures for the molecular mechanics/dynamics. No explicit bonding force constant or geometric constraint was used for the distance between the Ni-atom and the potentially coordinating N-atom. Therefore, the only component of the force field that favored short Ni–ligand distances was the *Coulomb* attraction of partial charges as included in the treatment of nonbonded interactions.

Two different methods for conformational search were used: 1) high-temperature molecular dynamics with simulated annealing, and 2) a systematic variation of all

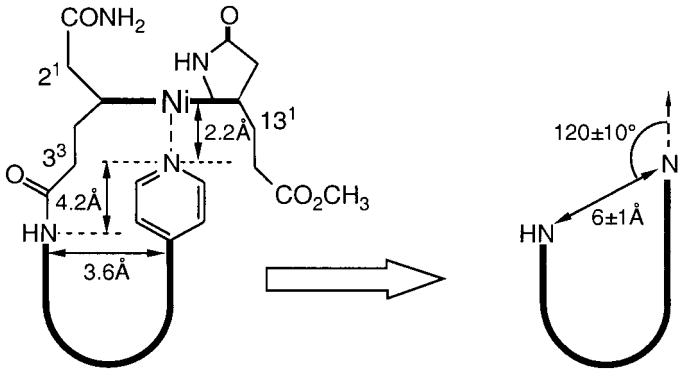

Fig. 2. *Schematic illustration of the geometric constraints derived for the spacer–ligand assembly*

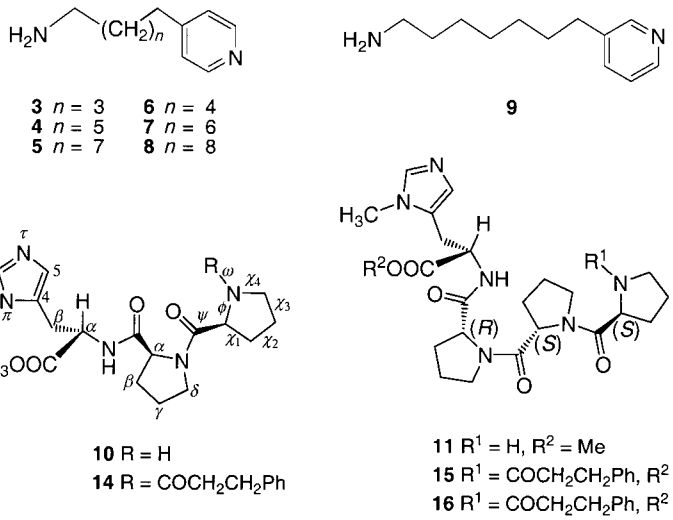

torsional angles about freely rotating single bonds in steps of 60 degrees with subsequent minimizations. Each run typically produced 1000 minimized structures that were analyzed by means of *Perl* routines as follows. The dihedral angles around (unrestrained) single bonds were grouped into the categories p (g^+), m (g^-), or t, and a conformational code was generated by concatenation of these letters into a string (*e.g.*, pttmmtpt). If two structures had the same conformational code and their energies were the same within 4 kcal/mol, they were considered identical and the duplicate with the higher energy was eliminated from the set. The remaining conformers were analyzed geometrically by using the criteria discussed above (*Fig. 2*) and classified into 'able to coordinate' and 'unable to coordinate'. Finally, their relative energies were used for a rough estimate of the molar fractions of 'coordinating' and 'non-coordinating' conformers.

Out of the *ca.* 50 structures examined, two families of spacer–ligand constructs, namely the pyridinalkanamines **3**–**9** and the proline-containing peptides **10** and **11** with a C-terminal N^{π}-methyl-L-histidine, emerged as particularly promising candidates having low-energy conformers with the required geometry (see *Tables 1* and *2*). The pyridinalkanamines **3**–**9** with their long flexible chains on one hand, and the peptides **10** and **11** containing two or even three neighboring proline units on the other hand, represent two extreme cases with respect to conformational flexibility. Conformational search methods such as those used here do not provide thermodynamic ensembles but a (not necessarily complete) list of conformers and their relative energies. The entropic term of the intramolecular complexation equilibrium is expected to be much more favorable for the rigid peptide linkers of **10** and **11** than for the flexible alkane chains of **3**–**9**. In other words, although both classes have low-energy conformers with the right shape, the total number of predicted low-energy conformers is much lower for the peptide linkers, and they should, therefore, be better preorganized for complexation than the alkane linkers of the alkanamines. Since we planned to eventually investigate the weakly coordinating native carboxamide ligand using the same linkers, we opted for the more-rigid peptide linkers as our targets. Because the calculations predicted that **10** and **11** have similar propensities for coordination, we decided to synthesize both molecules and to base our final selection on the experimentally determined NMR-solution conformation of their *N*-acylated derivatives.

Table 1. *HTD Simulation of 3³,8³,12²,18²-Tetra-*O*-methyl-13³-***L***-F 430* (**L** = ligand derived from **3**–**11**): *Comparison of the Structure with the Lowest Energy Overall and the Coordinating Structure of Lowest Energy*

Ligand **L** derived from	Lowest energy overall		Lowest energy coordinating		ΔE[a]) [kcal/mol]	n_{coord}[b])	x_{coord}[c])
	d(Ni–N) [Å]	coord. angle [°]	d(Ni–N) Å]	coord. angle [°]			
3	8.6	58.0	2.9	160.7	0.0	3	0.398
4	8.7	73.4	–	–	–	0	0
5	3.7	81.5	2.9	155.6	6.0	2	$< 10^{-4}$
6	8.3	59.8	–	–	–	0	0
7	7.4	117.5	2.8	147.1	3.1	2	0.014
8	3.0	126.1	3.0	126.1	0.0	1	0.941
9	6.2	142.5	3.0	159.7	2.7	2	0.006
10	6.3	96.5	3.5	147.0	2.2	1	$< 10^{-3}$
11	3.6	116.6	2.9	170.1	3.4	2	0.003

[a]) $\Delta E = E(1^{st}$ coord. structure) – E(structure with lowest energy). [b]) Number of coordinating structures found after elimination of duplicate conformers. [c]) Estimated molar fraction of coordinating conformers.

Synthesis of Two Proline-Containing Peptide Loops. – Peptide **10** was synthesized in solution as shown in *Scheme 2* by coupling of N^{π}-methyl-L-histidine methyl ester **12** and commercial Fmoc-Pro-Pro-OH (Fmoc = (9*H*-fluoren-9-ylmethoxy)carbonyl) (→ **13**). For the determination of the NMR-solution conformation, peptide **10** was acylated at the N-terminus with benzenepropanoic acid (PpOH) (as a model for the propanoic acid side chain of coenzyme F 430) to give **14**.

Initial attempts to synthesize tetrapeptide **11** by solution methods failed because deprotection of the intermediate Fmoc-Pro-His(π-Me)-OMe led to the formation of

Table 2. *Torsional Analysis of 3³,8³,12²,18²-Tetra-*O*-methyl-13³-***L*** (***L*** = ligand derived from **10** or **11**): Comparison of the Structure with the Lowest Energy Overall and the Coordinating Structure with the Lowest Energy*

Ligand **L** derived from	Lowest energy overall		Lowest energy coordinating		ΔE[a]) [kcal/mol]	n_{coord}[b])	x_{coord}[c])
	d(Ni–N) [Å]	coord. angle [°]	*d*(Ni–N) [Å]	coord. angle [°]			
10	3.6	118.4	2.9	163.4	7.7	1	$< 10^{-4}$
11	6.3	87.1	3.0	156.5	6.5	1	$< 10^{-4}$

[a]) [b]) [c]) See *Table 1*.

Scheme 2. *Synthesis of Tripeptide* **10** *and of its N-Terminal 3-Phenylpropanoyl-Substituted Derivative* **14**

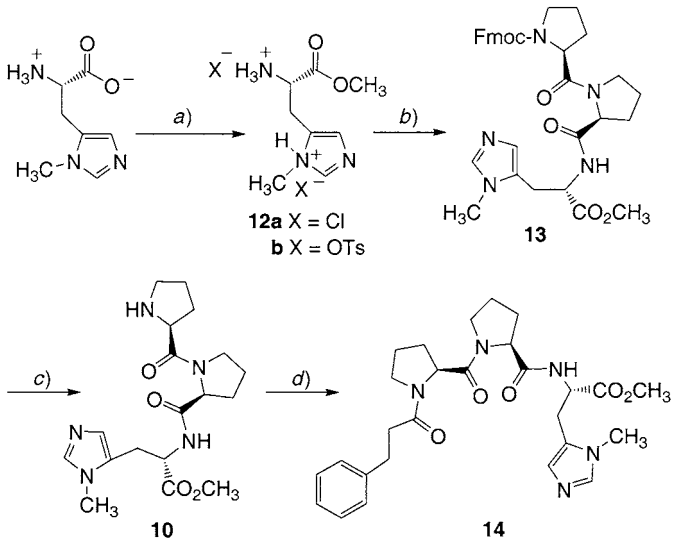

a) MeOH, anh. HCl. *b*) Fmoc-Pro-Pro-OH, HBTU (=2-(1*H*-benzotriazol-1-yl)-1,1,3,3-tetramethyluronium hexafluorophosphate), HOBt (=1-hydroxy-1*H*-benzotriazole), DMF, $^{i}Pr_2NEt$. *c*) Piperidine, DMF. *d*) Benzenepropanoic acid, HBTU, HOBt, $^{i}Pr_2NEt$, DMF.

the diketopiperazine derivative as the major product. However, synthesis on solid support according to slightly modified literature procedures [27–30] (for details, see *Exper. Part*) allowed us to prepare pure tetrapeptide **15**, although in low yield. For the purpose of the NMR study, its N-terminus was acylated with the 3-phenylpropanoyl group (Pp). Finally, esterification gave **16**.

^{1}H-NMR Study of the Solution Conformation of N-Acylated Peptidic Spacer–Ligand Structures. – In the ^{1}H-NMR spectra of **14** and **16** in CD_3CN (with 5–10 µl of CF_3COOH added to protonate the histidine moiety), as well as in the ^{1}H-NMR spectra of the starting material (Fmoc-Pro-Pro-OH) and the intermediates **10** and **13**, two or three signals with different integrals could be observed for most protons. Exchange cross-peaks correlating the signals attributed to the same proton in ROESY experiments with long mixing times demonstrated that the subspectra correspond to slowly

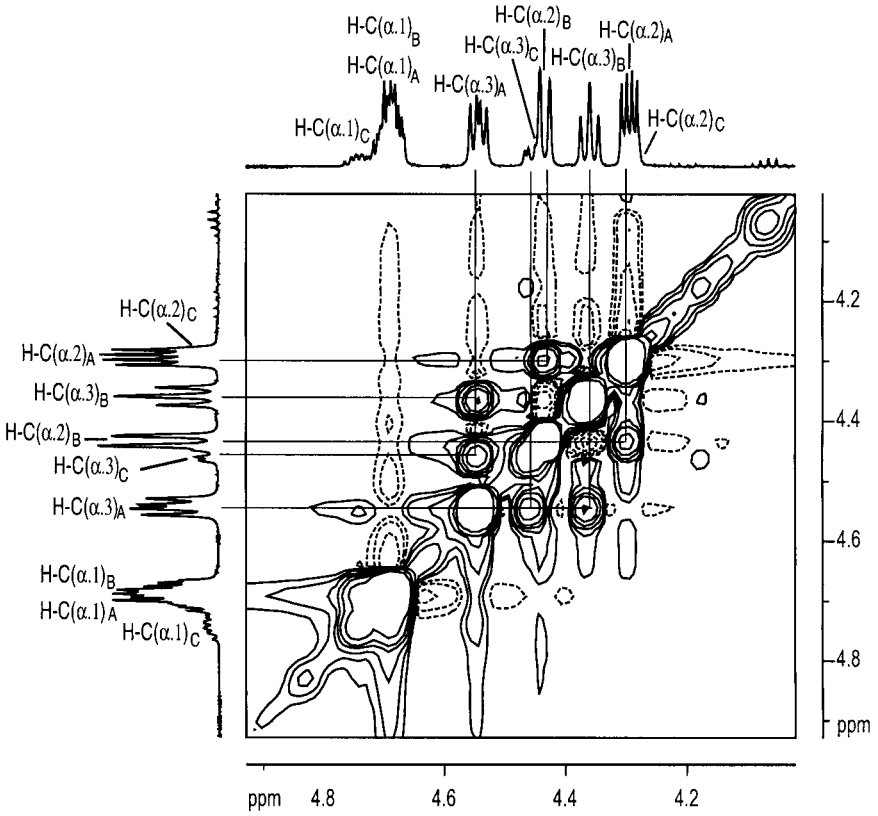

Fig. 3. *Expansion of the ROESY plot* (H–C(α) region) *of tripeptide* **14** *showing the exchange peaks connecting corresponding protons in the three conformers* (**A**–**C**)

interconverting conformers. *Fig. 3* illustrates this for the *N*-acylated compound **14**. The observed dynamic exchange is due to *cis*/*trans* isomerization of proline secondary-amide bonds, a frequently observed and well-studied process in proline-containing peptides [31–33].

Fortunately, at room temperature, the rates of exchange between the conformers were so low that the NOEs of the major conformers **14A** and **14B**, as well as **16A**, could be used as restraints in the structure calculations without explicitly taking into account the influence of exchange on the NOE intensities. For each conformer, the ROESY cross-peak volumes were normalized on the basis of the molar fractions determined by integration in the 1D spectrum. The known distance between the N^{τ}-Me group and H–C(2) at the histidine aromatic ring (in the case of **14A** and **16A**) or the distance between the two aromatic histidine protons H–C(5) and H–C(2) (in the case of **14B**) were used for calibration, and upper and lower distance restraints were derived from the NOEs as listed in *Tables 9–11* (see below, *Exper. Part*). The puckering of the proline ring (specified by torsional angles χ_1, χ_2, χ_3, and χ_4) is known to be coupled to the *cis*/*trans* configuration of the amide bond [34][35]. In principle, the four

conformations *cis*-DOWN and *trans*-DOWN (C(γ)-*exo*, χ_1 and χ_3 positive and χ_2 and χ_4 negative) and *cis*-UP and *trans*-UP (C(γ)-*endo*, χ_1 and χ_3 negative, χ_2 and χ_4 positive) are possible for each proline unit[3]). Analysis of coupling constants and NOEs allowed us to assign a sufficient number of the diastereotopic C–H_2(β), C–H_2(γ), and C–H_2(δ) protons to deduce the puckering of the proline rings in all conformers.

Of the four *cis*/*trans* isomers that are possible for the tripeptide Pp-Pro-Pro-His(π-Me,H^+)-OMe (**14**; Pp = 3-phenylpropanoyl = 1-oxo-3-phenylpropyl), the ^{1}H-NMR spectra showed only three in a ratio of 5:4:1. The relative volumes of the exchange peaks between the three conformers **14A**, **14B**, and **14C** indicate that they interconvert according to the specific sequence consistent with the final assignments **14B** = Pp-*trans*-UP-Pro-*cis*-DOWN-Pro-*trans*-His(π-Me,H^+)-OMe, **14A** = Pp-*trans*-UP-Pro-*trans*-UP-Pro-*trans*-His(π-Me,H^+)-OMe, and **14C** = Pp-*cis*-DOWN-Pro-*trans*-UP-Pro-*trans*-His(π-Me,H^+)-OMe, which resulted from the complete analysis of the ^{1}H-NMR data. For the minor conformer **14C**, strong overlap and the low signal-to-noise ratio of ROESY cross-peaks prevented a full structure calculation, but qualitative analysis of the NOE pattern still allowed the unequivocal assignment of Pp-*cis*-DOWN-Pro- *trans*-UP-Pro-*trans*-His(π-Me,H^+)-OMe to **14C**. Fifty structures that do not violate any of the ^{1}H-NMR-derived restraints (*Tables 9* and *10*, see *Exper. Part*) were generated for each of the conformers **14A** and **14B** by torsional-angle dynamics according to a simulated annealing protocol with the program DYANA [36]. *Fig. 4*,*a* and *b*, show bundles with the eight structures of lowest energy for conformers **14A** and **14B**, respectively.

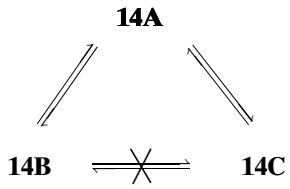

The ^{1}H-NMR spectra of Pp-Pro-Pro-D-Pro-His(π-Me,H^+)-OMe (**16**) in CD_3CN (with *ca.* 10 µl of CF_3COOH) indicated the presence of two slowly interchanging conformers in a 9:1 ratio. All δ(H) and δ(C) of the major conformer **16A** and most signals of the minor conformer **16B** could be assigned by using 2D-NMR techniques. However, only the NOE intensities of conformer **16A** were reliable enough for the derivation of structural restraints (*Table 11*, see *Exper. Part*). A bundle of the six structures lowest in energy and consistent with the ^{1}H-NMR restraints, calculated for

---

[3]) Nomenclature of proline-puckering conformations according to [34].

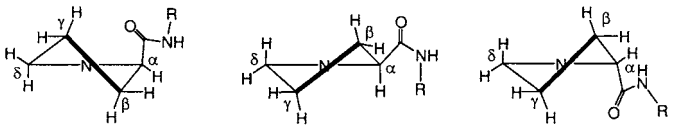

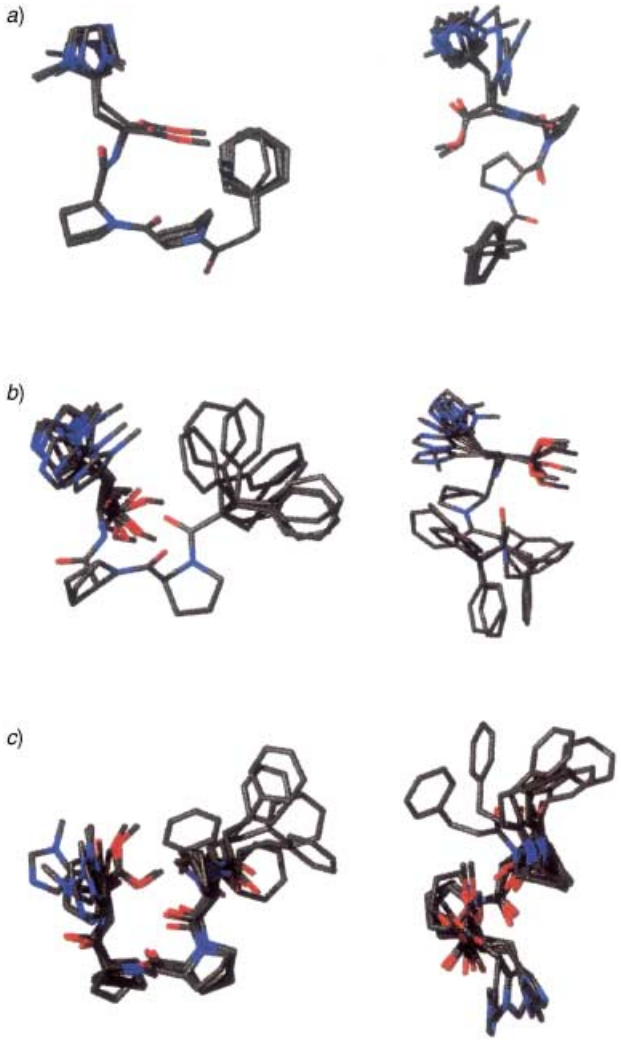

Fig. 4. *NMR-Derived structures for the acylated peptides* **14** *and* **16**: a) *conformer* **14A**, b) *conformer* **14B**, *and* c) *conformer* **16A**. Shown are bundles of the eight structures for **14A** and **14B** and the six structures for **16A** with the lowest energy that do not violate any NMR-derived constraints.

conformer **16A** with the procedures described above for the tripeptide **14**, are displayed in *Fig. 4*, *c*. They show that the preferred conformation **16A** of the protonated tetrapeptide in solution is Pp-*trans*-UP-D-Pro-*trans*-UP-Pro-*trans*-UP-Pro-*trans*-His(π-Me,H^+)-OMe.

Refinement of the Molecular Modeling. – In a final step of the selection process, we subjected the F 430 macrocycle with the peptide loops **10** or **11** attached to the side chain at C(3) or C(13) of coenzyme F 430 to high-temperature molecular-dynamics calculations under the restraints derived from the NMR data of the unattached

acylated model peptides **14** and **16** (for methods, see *Exper. Part*). For conformers **10A** and **10B** of the tripeptide derivative, structures that fulfilled the geometric requirements for coordination were predicted to be either lowest in energy or only slightly above the conformer with the lowest energy (see *Tables 3* and *4*). The all-*trans* tripeptide **10A** was best preorganized for coordination when attached to the side chain at C(13) (*Fig. 5, a*) whereas the conformer **10B** gave the best coordination geometry when attached to C(3^3) (*Fig. 5, b*). Since the two almost isoenergetic conformers were found to interconvert at room temperature, it was reasonable to assume that the peptide would adjust its conformation to allow optimal coordination to the Ni-atom when attached to either C(3^3) or C(13^3). In contrast to the tripeptide **10**, no low-energy conformations with the correct shape for coordination were predicted for tetrapeptide **11** attached to either C(3^3) or C(13^3) of F 430 when experimentally derived restraints for conformer **11A** were applied during the simulated annealing protocol.

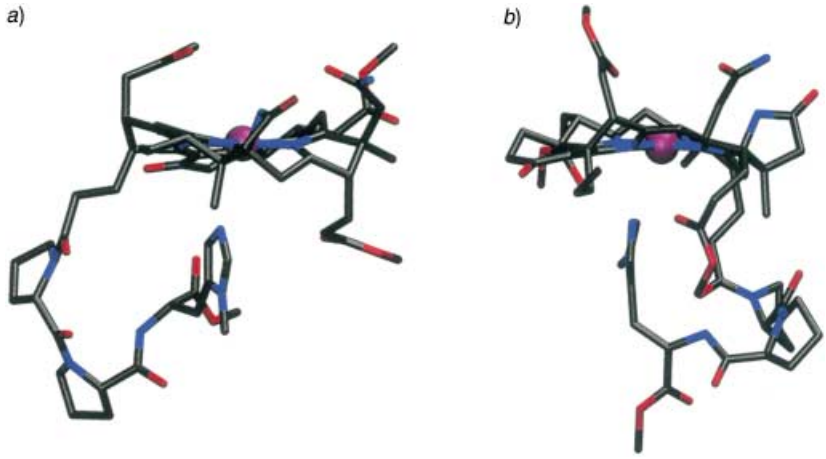

Fig. 5. *Molecular modeling refined with NMR-derived restraints: Typical low-energy structures of tripeptide* **10** *linked to propanoic acid side chains of F 430.* a) **10A** *attached to C(13^3) and* b) **10B** *attached to C(3^3)*

Conclusions. – From an initial set of *ca.* 50 structures, our selection procedure singled out tripeptide **10** as the most-promising spacer–ligand combination for the construction of a derivative of coenzyme F 430 exhibiting intramolecular coordination from the α-face of the macrocycle. The initial set of structures that were included in the computer-assisted conformational search is of course far from complete, as it depended on imagination and chemical intuition. The experimental determination of the actual solution structure of the most-promising spacer–ligand molecules provided an additional degree of confidence in view of the uncertainties introduced by the force field, the neglect of explicit solvent, and the incompleteness of conformational search procedures. Of course, this approach depends on the assumption that, once attached, the spacer–ligand will be only moderately influenced in its conformation by specific nonbonded interactions with the hydrocorphin. The final test of this hypothesis, the synthesis of a corresponding derivative of coenzyme F 430 and the proof that it is forming an intramolecular axial complex will be described in *Part II* [26a].

Table 3. *HTD Simulation of 3³,8³,12²,18²-Tetra-*O*-methyl-13³-***L****-F 430 and 8³,12²,13³,18²-Tetra-*O*-methyl-3³-***L*** - F 430* (**L** = ligand derived from **10A**) *with NMR-Derived Restraints: Comparison of the Structure with the Lowest Energy Overall and the Coordinating Structure of Lowest Energy*

10A bound to	Rs[d])	T_{sim} [K]	Lowest energy overall		Lowest energy coordinating		ΔE[a]) [kcal/mol]	n_{coord}[b])	x_{coord}[c])
			d(Ni–N) [Å]	coord. angle [°]	d(Ni–N) [Å]	coord. angle [°]			
C(13³)	*A*	298	2.75	146.7	2.75	146.8	0	16	0.78
C(13³)	*A*	400	2.8	148.3	2.8	148.3	0	20	0.77
C(13³)	*B*	400	6.4	98.1	2.9	158.3	0.32	6	0.3329
C(13³)	*B*	700	5.8	115.5	3.0	125.9	3.23	8	0.0013
C(13³)	*B*	1000	2.9	157.8	2.9	157.8	0	3	0.9621
C(3³)	*A*	298	6.3	145.6	–	--	--	0	0
C(3³)	*A*	400	6.3	145.9	–	--	--	0	0
C(3³)	*B*	400	9.8	53.7	–	–	–	0	0
C(3³)	*B*	700	9.9	54.9	–	–	–	0	0
C(3³)	*B*	1000	9.7	28.8	2.9	171.7	-7.81	3	$< 10^{-4}$

[a]) [b]) [c]) See *Table 1*. [d]) *A:* taking into account all NMR-derived restraints; *B:* only intra-peptide restraints.

Table 4. *HTD Simulation of 3³,8³,12²,18²-Tetra-*O*-methyl-13³-***L****-F 430 and 8³,12²,13³,18²-Tetra-*O*-methyl-3³-***L*** - F 430* (**L** = ligand derived from **10B**) *with NMR-Derived Restraints: Comparison of the Structure with the Lowest Energy Overall and the Coordinating Structure of Lowest Energy*

10B bound to	Rs[d])	T_{sim} [K]	Lowest energy overall		Lowest energy coordinating		ΔE[a]) [kcal/mol]	n_{coord}[b])	x_{coord}[c])
			d(Ni–N) [Å]	coord. angle [°]	d(Ni–N) [Å]	coord. angle [°]			
C(13³)	A	298	3.3	126.5	–	–	–	0	0
C(13³)	*A*	400	6.9	128.3	–	–	–	0	0
C(13³)	*B*	400	3.0	147.4	3.0	147.4	0	4	0.52
C(13³)	*B*	700	3.0	145.4	3.0	145.4	0	7	0.054
C(13³)	*B*	1000	2.9	139.2	2.9	139.2	0	6	0.65
C(3³)	*A*	298	3.2	154.6	2.8	162.8	0	2	$< 10^{-4}$
C(3³)	*A*	400	2.7	128.2	2.7	128.2	0	4	1.0
C(3³)	*B*	400	8.2	43.7	–	–	–	0	0
C(3³)	*B*	700	4.5	115.6	2.9	149.0	−6.07	8	$< 10^{-4}$
C(3³)	*B*	1000	4.55	120.9	2.9	141.7	−9.68	6	$< 10^{-4}$

[a]) [b]) [c]) See *Table 1*. [d]) *A:* taking into account all NMR-derived restraints; *B:* only intra-peptide restraints.

We thank Ms. *B. Brandenberg* for acquiring the 2D-NMR spectra and Ms. *B. Bergamasci*, Biochemistry, University of Zürich, for help with the solid-phase synthesis of peptides. This work was supported by grant 2000-006773 of the *Swiss National Science Foundation*.

Experimental Part

1. *General*. Abbrevations: DMF = dimethylformamide, DMPU = 3,4,5,6-tetrahydro-1,3-dimethylpyrimidin-1(2*H*)-one, HBTU = 2-(1*H*-benzotriazol-1-yl)-1,1,3,3-tetramethyluronium hexafluorophosphate, HOBt = 1-hydroxy-1*H*-benzotriazole; h.v. = high vacuum (0.001–0.1 Torr). Solvents for extractions were distilled. $^{i}Pr_2NEt$ and DMPU were distilled over CaH_2 and stored under N_2 at −20°. DMF was freshly distilled over CaH_2

at 40°/*ca.* 10 mbar over a fractionating column (110 cm) packed with glass beads, by using a reflux ratio of 10:1 and taking the middle 30%. Distilled DMF was stored under N_2 at −20°. MeOH was distilled over Mg under N_2. All reagents were purchased either from *Bachem*, *Novabiochem*, or *Fluka* in highest available quality and were used without further purification. Commercially available N^2-[(9*H*-fluoren-9-yl-methoxy)carbonyl]-L-prolyl-L-proline (*Bachem*; ee 99.7%) showed two conformers in slow exchange in the NMR spectra; for full δ(H) and δ(C) assignments of both conformers, see [37]. *C-18* Cartridges (*Sep-Pak*) were washed with at least 50 ml of MeOH or MeCN. TLC: *Merck* silica gel *60* F_{254}, UV detection or development with ninhydrin or mostain solns. under heating. Flash chromatography (FC): *Fluka* silica gel *60* (40–63 μm). HPLC: solvent systems were degassed in the vacuum before use; anal. reversed-phase column, *Nucleosil 50-5 C18AB*, 250 × 4 mm with pre-column (*Macherey-Nagel*); prep. reversed-phase column, *Nucleosil 50-5 C18AB*, 250 × 10 mm including pre-column (*Macherey-Nagel*). Optical rotation: *Perkin-Elmer 241* polarimeter (10 cm, 1 ml). M.p.: *Büchi 510*; uncorrected. UV/VIS: *Lambda-20* spectrophotometer (*Perkin-Elmer*). NMR Spectra: atom labels according to the IUBMB-IUPAC convention for peptides [38]; *Bruker DRX-500* and *DRX-400* spectrometers, at 26.7°; DQF-COSY, HSQC, and HMBC with gradients for coherence pathways selection; ROESY, offset compensated [39], assignments marked with * are based on the HMBC, HSQC, DQF-COSY, and ROESY and were performed with the aid of the program SPARKY [40], which also served as the tool for volume integration of ROESY cross-peaks. MS: ESI, *TSQ 7000* (*Finnigan*); HR-MALDI, *Ionspec 4.7T FTICR-MS*, N_2-laser (337 nm), matrix 2,5-DHB (2,5-dihydroxybenzoic acid). Elemental analysis was performed by the Microanalytical Laboratory, ETH-Zürich.

2. *Syntheses.* N^π-*Methyl*-L-*histidine Methyl Ester Salts* **12**. The hygroscopic hydrochloride **12a** was prepared in quant. yield from N^π-methyl-L-histidine (400 mg, 2.36 mmol) following a known procedure [41] and stored under N_2 ($[\alpha]_{20}^{D} = +11.6$ ($c = 1$, H_2O); m.p. 207° ([41]: m.p. 208–209°). Equal results in the next step were obtained with the 4-methylbenzenesulfonate **12b**, which was easier to handle because it is not hydroscopic.

4-Methylbenzenesulfonate **12b**: N^π-Methyl-L-histidine (338 mg, 2 mmol) and 4-methylbenzenesulfonic acid (1.14 g, 6 mmol) were kept under reflux in abs. MeOH (10 ml) for 24 h, the solvent was evaporated and the residue recrystallized from Et_2O/acetone 1:1: **12b** (470 mg, 45%). M.p. 110–112°. ^{1}H-NMR (400 MHz, CD_3OD): 8.82 (*d*, $J = 0.8$, 1 H); 7.63 (*m*, 4 H); 7.46 (*m*, 1 H); 4.44 (*t*, $J = 7.1$, 1 H); 3.83 (*s*, 3 H); 3.80 (*s*, 3 H); 3.43 (*ddd*, $J = 0.9$, 7.0, 16.2, 1 H); 3.28 (*ddd*, $J = 0.7$, 7.3, 16.2, 1 H); 2.31 (*s*, 6 H). ^{13}C-NMR (100 MHz, CD_3OD): 169.4; 143.4; 141.8; 137.8; 130.2; 129.9 (2 C); 126.9 (2C); 120.45; 54.2; 52.3; 34.1; 25.1; 25.1. ESI-MS (Q + 1): 184.3 (*M*H$^+$, 100), 185.9 (9). Anal. calc. for $C_{22}H_{29}N_3O_8S_2$ (527.62): C 50.08, H 5.54, N 7.96, O 24.26, S 12.16; found: C 49.88, H 5.61, N 7.85, O 24.54, S 12.05.

N^α-*[(9*H-*Fluoren-9-ylmethoxy)carbonyl]*-L-*prolyl*-L-*prolyl*-N^π-*methyl*-L-*histidine* (**13**). The clear soln. obtained by addition of ^{i}Pr$_2$NEt (0.88 ml, 5.13 mmol) to a suspension of **12a** (314 mg, 1.22 mmol), Fmoc-Pro-Pro-OH (523 mg, 1.22 mmol), HBTU (509 mg, 1.34 mmol), and HOBt (181 mg, 1.34 mmol) in DMF (10 ml) at 0° was stirred for 2 h at 0° and then for 1 h at 25°. The solvent was evaporated at 25°, the residue dissolved in 0.5M aq. $NaHCO_3$ (20 ml) and extracted with AcOEt (5 × 50 ml), and the org. phase dried ($MgSO_4$) and concentrated to an oil, which was taken up in CH_2Cl_2 (1–2 ml). The product was precipitated by adding slowly and dropwise the CH_2Cl_2 soln. into cold stirred Et_2O (150 ml). The precipitate was filtered off, washed with Et_2O, and dried over P_2O_5: **13** (683 mg, 93%). NMR: conformers **13A** (60%), **13B** (30%), and **13C** (10%) in slow exchange; for the major conformer **13A**, see below; for the other conformers, see [37]. **13A**: ^{1}H-NMR (500 MHz, CD_3CN/D_2O 9:1 (+ *ca.* 10 μl of CF_3COOD)): 8.51 (*s*, 1 H, H–C(5.3); 7.84 (*m*, 2 H, H–C(4.Fmoc), H–C(5.Fmoc)); 7.67 (*m*, 2 H, H–C(1.Fmoc), H–C(8.Fmoc)); 7.44 (*m*, 2 H, H–C(3.Fmoc), H–C(6.Fmoc)); 7.36 (*m*, 2 H, H–C(2.Fmoc), H–C(7.Fmoc)); 7.23 (*s*, 1 H, H–C(2.3)); 4.73 (*dd*, $J = 4.6$, 9.9, 1 H, H–C(α.3)); 4.65 (*dd*, $J = 5.3$, 10.9, 1 H, H′–C(α.Fmoc); 4.44 (*dd*, $J = 5.1$, 10.9, 1 H, H″–C(α.Fmoc); 4.18 (*t*, $J = 5.1$, 1 H, H–C(9.Fmoc)); 4.10 (*dd*, $J = 3.9$, 8.8, 1 H, H–C(α.2)); 4.07 (*dd*, $J = 3.6$, 8.8, 1 H, H–C(α.1)); 3.77 (*s*, 3 H, Me(N^π.3)); 3.73 (*s*, 3 H, Me(*O*.3)); 3.42 (*m*, 1 H, H′–C(δ.1); 3.33 (*m*, 1 H, H″–C(δ.1)); 3.32 (*m*, 1 H, H′–C(δ.2)); 3.25 (*m*, 1 H, H′–C(β.3)); 3.07 (*m*, 1 H, H″–C(β.3)); 2.98 (*m*, 1 H, H″–C(δ.2)); 2.22 (*m*, 2 H, CH_2(γ.2)); 2.11 (*m*, 1 H, H′–C(β.1)); 2.06 (*m*, 1 H, H′–C(β.2)); 1.82 (*m*, 1 H, H″–C(β.2)); 1.77 (*m*, 1 H, H″–C(β.1)). ^{13}C-NMR (125 MHz, CD_3CN/D_2O 9:1 (+ *ca.* 10 μl of CF_3COOD)): 172.79 (CO(.2)); 172.64 (CO(.2)); 172.05 (CO(.3)); 156.07 (OCON(Fmoc)); 145.30, 144.88 (C(8a.Fmoc), C(9a.Fmoc)); 142.20, 142.10 (C(4a.Fmoc), C(4b.Fmoc)); 136.01 (C(3.3)); 131.66 (C(1.3)); 128.76, 128.72 (C(3.Fmoc), C(6.Fmoc)); 128.25 (C(2.Fmoc), C(7.Fmoc)); 125.75, 125.60 (C(1.Fmoc), C(8.Fmoc)); 120.93 (C(4.Fmoc), C(5.Fmoc)); 120.91 (C(2.3)); 67.11 (CH_2(α.Fmoc)); 60.70 (C(α.2)); 58.85 (C(α.1)); 53.69 (Me(*O*.3)); 51.32 (C(α.3)); 48.25 (C(9.Fmoc)); 48.12 (C(δ.1)); 47.67 (C(δ.2)); 34.32 (Me(N^π.3)); 30.67 (C(β.1)); 29.80 (C(β.2)); 25.98 (C(β.3)); 25.43 (C(γ.2)); 23.88 (C(γ.1)). ESI-MS (Q + 1): 600.2 (100, *M*H$^+$, $C_{33}H_{38}N_5O_6^+$), 601.2 (38), 602.2 (8), 603.2 (2).

L-*Prolyl*-L-*prolyl*-N$^{\pi}$-*methyl*-L-*histidine Methyl Ester* (**10**). Piperidine (2.0 ml, 20 mmol) was added to a soln. of **13** (704 mg, 1.2 mmol) in DMF (5 ml), and the mixture was stirred at 25° under N_2 for 1 h. The solvent was evaporated, the residue dissolved in MeCN (10 ml), and the soln. extracted with hexane (3 × 20 ml). The MeCN phase was evaporated, the residue taken up in CH_2Cl_2 (1 ml), and the soln. added dropwise to cold stirred Et_2O (150 ml). The precipitate was collected by centrifugation, washed with Et_2O and dried over P_2O_5: **10** (246 mg, 55%). NMR: conformers **10A** (90%), and **10B** (10%) in slow exchange; for the major conformer **10A**, see below, for the other conformer, see [37]. **10A**·H$^+$: ^{1}H-NMR (500 MHz, CD_3CN + 5 µl of CF_3COOH)*: 8.384 (*d*, *J* = 0.7, 1 H, H–C(2.3); 7.865 (br. *s*, 1 H, H′–N(α.1)); 7.750 (br. *s*, 1 H, H″–N(α.1)); 7.269 (*dd*, *J*(H′–C(β.3), H–C(5.3)) = 1.3, *J*(H″–C(β.3), H–C(5.3)) = 0.7, 1 H, H–C(5.3); 7.044 (br. *s*, 1 H, H–N(α.3)); 4.779 (*ddd*, *J*(H–N(α.3), H–C(α.3)) = 1.3, *J*(H′–C(β.3), H–C(α.3)) = 4.2, *J*(H″–C(β.3), H–C(α.3) = 10.4, 1 H, H–C(α.3)); 4.427 (*d*, *J*(H–C(β.1), H–C(α.1)) = 7.5, 1 H, H–C(α.1)); 4.288 (*dd*, *J*(H′–C(β.2), H–C(α.2)) = 8.5, *J*(H″–C(β.2), H–C(α.2)) = 5.4, 1 H, H–C(α.2)); 3.779 (*d*, *J*(H–C(2.3), Me(*N*$^{\pi}$.3)) = 0.5, 3 H, Me(*N*$^{\pi}$.3)); 3.73 (*s*, 3 H, Me(*O*.3)); 3.549 (*ddd*, *J*(H′–C(γ.2), H′–C(δ.2)) = 7.0, *J*(H″–C(γ.2), H′–C(δ.2)) = 7.0, *J*(H″–C(δ.2), H′–C(δ.2)) = 9.9, 1 H, H′–C(δ.2)); 3.478 (*m*, *J*(H–N(α.1), H′–C(δ.1)) = 6.14, *J*(H′–C(γ.1), H′–C(δ.1)) = 6.9, *J*(H″–C(γ.1), H′–C(δ.1)) = 6.95, *J*(H″–N(α.1), H′–C(δ.1)) = 16.75, 1 H, H′–C(δ.1)); 3.474 (*ddd*, *J*(H′–C(δ.2), H″–C(δ.2)) = 9.9, *J*(H′–C(γ.2), H″–C(δ.2)) = 6.8, *J*(H″–C(γ.2), H″–C(δ.2)) = 6.8, 1 H, H″–C(δ.2)); 3.325 (*m*, *J*(H–N(α.1), H″–C(δ.1)) = 6.0, *J*(H″–N(α.1), H″–C(δ.1)) = 6.06, *J*(H′–C(δ.1), H″–C(δ.1)) = 12.04, *J*(H′–C(γ.1), H–C(δ.1)) = 7.04, *J*(H″–C(γ.1), H″–C(δ.1)) = 7.04, 1 H, H″–C(δ.1)); 3.257 (*dd*, *J*(H–C(5.3), H′–C(β.3)) = 0.9, *J*(H′–C(α.3), H′–C(β.3)) = 4.2, *J*(H″–C(β.3), H′–C(β.3)) = 15.9, 1 H, H′–C(β.3)); 3.035 (*ddd*, *J*(H–C(5.3), H″–C(β.3)) = 0.9, *J*(H′–C(α.3), H″–C(β.3)) = 4.2, *J*(H′–C(β.3), H″–C(β.3)) = 15.9, 1 H, H″–C(β.3)), 2.457 (*dddd*, *J*(H–C(α.1), H′–C(β.1)) = 7.4, *J*(H″–C(γ.1), H′–C(β.1)) = 8.8, *J*(H′–C(γ.1), H′–C(β.1)) = 8.8, *J*(H″–C(β.1), H′–C(β.1)) = 13.0, 1 H, H′–C(β.1)); 2.198 (*dddd*, *J*(H″–C(γ.2), H′–C(β.2)) = 7.0, *J*(H″–C(β.2), H′–C(β.2)) = 7.0, *J*(H–C(α.2), H′–C(β.2)) = 8.4, *J*(H′–C(γ.2), H′–C(β.2)) = 12.6, 1 H, H′–C(β.2)); 2.039 (*ddd*, *J*(H′–C(δ.1), H′–C(δ.1)) = 6.5, *J*(H″–C(δ.1), H′–C(δ.1)) = 6.5, *J*(H″–C(γ.1), H′–C(δ.1)) = 14.0, 1 H, H′–C(γ.1)); 1.985 (*m*, 1 H, H′–C(γ.2)); 1.937 (*m*, 1 H, H″–C(γ.2)); 1.916 (*m*, 1 H, H″–C(γ.1)); 1.884 (*m*, 1 H, H″–C(β.1)); 1.838 (*ddd*, *J*(H″–C(γ.2), H″–C(β.2)) = 7.1, *J*(H′–C(β.2), H″–C(β.2)) = 7.1, *J*(H′–C(γ.2), H″–C(β.2)) = 12.6, 1 H, H″–C(β.2)). ^{13}C-NMR (125 MHz, CD_3CN + *ca.* 4 µl of CF_3COOH): 172.13 (CO(.2)), 171.50 (CO(.3)); 167.89 (CO(.1)); 135.96 (C(2.3)); 131.70 (C(4.3)); 119.64 (C(5.3)); 61.49 (C(α.2)); 60.40 (C(α.1)); 53.47 (Me(*O*.3)); 51.27 (C(α.3)); 48.22 (C(δ.2)); 48.12 (C(δ.1)); 34.47 (Me(*N*$^{\pi}$.3)); 30.12 (C(β.2)); 29.52 (C(β.1)); 26.52 (C(β.3)); 25.69 (C(γ.2)); 25.21 (C(γ.1)). ESI-MS (Q + 1): 378.3 (100, *M*H$^+$, $C_{18}H_{28}N_5O_4^+$), 379.3 (18), 380.3 (3).

N$^{\alpha}$-*(1-Oxo-3-phenylpropyl)*-L-*prolyl*-L-*prolyl*-N$^{\pi}$-*methyl*-L-*histidine Methyl Ester* (**14**). Under N_2, **13** (40 mg, 0.11 mmol), benzenepropanoic acid (18 mg, 0.12 mmol), HBTU (42 mg, 0.11 mmol), and HOBt (15 mg, 0.11 mmol) were suspended in DMF (2 ml) at 0°, ^{i}Pr$_2$NEt (51 µl, 0.22 mmol) was added, and the soln. was kept at 0° for 2 h followed by 1 h at 25°. After evaporation, the residue was dissolved in 0.1M aq. $NaHCO_3$ (5 ml), the soln. extracted with AcOEt (6 × 5 ml), the combined org. phase dried ($MgSO_4$) and evaporated, and the crude product purified by CC (silica gel (3.4 g), CH_2Cl_2/MeOH 98:2 → 95:5): **14** (29 mg, 52%). NMR: conformers **14A** (52%), **14B** (38%), and **14C** (10%)[4]) in slow exchange: ^{1}H- and ^{13}C-NMR: *Tables 5* and *6*. ESI-MS (Q + 1): calc. for 510.4 (100, *M*H$^+$, $C_{27}H_{36}N_5O_5^+$), 511.4 (32), 512.4 (6).

Solid-Phase Synthesis of Tetrapetide **16**.

Immobilization of N$^{\pi}$-*Methyl*-L-*histidine*. Under N_2, N$^{\alpha}$-[(9*H*-fluoren-9-ylmethoxy)carbonyl]-N$^{\pi}$-methyl-L-histidine (392 mg, 1.0 mmol; 3× co-evaporated with abs. dioxane and dried under h.v.) and (2-chlorotrityl-chloride)-resin (1.0 g) were suspended in CH_2Cl_2 at 25°. DMPU (6 ml) and ^{i}Pr$_2$NEt (680 µl, 4.0 mmol) were slowly added, and the mixture was shaken for 1.5 h. Then the loaded resin was filtered, washed with CH_2Cl_2/MeOH/^{i}Pr$_2$NEt 17:2:1 (3 × 50 ml), CH_2Cl_2 (3 × 50 ml), DMF (3 × 50 ml), and again CH_2Cl_2 (2 × 20 ml), and dried under h.v. over KOH. To determine the resin's loading (max. theor. loading = $2.0 \cdot 10^{-3} - 3.2 \cdot 10^{-3}$ mmol), 2.0 mg of resin was treated with 20% piperidine/DMF (10.0 ml) for 0.5–1 h, and the UV adsorption of the supernatant soln. was measured (A_{298nm} = 0.83). Relative to the UV adsorption of a standard soln. of N$^{\alpha}$-[(9*H*-fluoren-9-ylmethoxy)carbonyl]glycine (30 mg, 0.1 mmol) in 20% piperidine/DMF (A_{298nm} = 1.21), the loading of the (2-chlorotrityl chloride)-resin with Fmoc-His(π-Me) was 68% ($1.36 \cdot 10^{-3} - 2.18 \cdot 10^{-3}$ mmol).

Solid-Phase Synthesis of N$^{\alpha}$*-(1-Oxo-3-phenylpropyl)*-L-*prolyl*-L-*prolyl*-D-*prolyl*-N$^{\pi}$-*methyl*-L-*histidine* (**15**) *and Capping*. The solid-phase synthesis of **15** was performed by sequential HBTU/HOBt coupling of Fmoc-D-

---

[4]) Relative integrals in the ^{1}H-NMR spectrum.

Table 5. *^{1}H-NMR Data* (500 MHz, CD_3CN/*ca.* 10 µl of CF_3COOH) *and Assignments for the Three Conformers of Tripeptide* **14**. δ(H) in ppm, *J* in Hz.

	δ(H)		
	14A	**14B**	**14C**
H−C(2.3)	8.361 ($J = 0.86$)	8.361	8.345
2 H_m	7.279	7.279	
H−C(5.3)	7.241	7.186	7.269
H−N(α.3)	7.240	8.863 (J(H−C(α.3), H−N(α.3)) = 8.3)	7.075 (J(H−C(α.3), H−N(α.3)) = 8.5)
2 H_P	7.227	7.230	7.172
H_o	7.187	7.269	7.237
H−C(α.3)	4.690	4.696 (J(H−N(α.3), H−C(α.3)) ≈ 8, J(H′−C(β.3), H−C(α.3)) ≈ 7.5, J(H″−C(β.3), H−C(α.3)) ≈ 7.5)	4.743 (J(H′−C(β.3), H−C(α.3)) = 4.5, J(H″−(β.3), H−C(α.3)) = 9.2)
H−C(α.1)	4.548 (J(H′−C(β.1), H−C(α.1)) = 5.2, J(H″−C(β.1), H−C(α.1)) = 8.3)	4.367 (J(H′−C(β.1), H−C(α.1)) = 7.3, J(H″−C(β.1), H−C(α.1)) = 7.3)	4.458 (J(H−C(β.1), H−C(α.1)) = 3.1, 8.8)
H−C(α.2)	4.301 (J(H″−C(β.2), H−C(α.2)) = 4.2, J(H′−C(β.2), H−C(α.2)) = 8.5)	4.435 (J(H′−C(β.2), H−C(α.2)) = 0, J(H″−C(β.2), H−C(α.2)) = 8.0)	4.293 (J(H−C(β.2), H−C(α.2)) = 8.5, 4.2)
Me(N^{π}.3)	3.762	3.760	3.761
Me(*O*.3)	3.710	3.649	3.710
H′−C(δ.2)	3.671	3.424	
H′−C(δ.1)	3.513	3.544 (J(H″−C(δ.1), H′−C(δ.1)) ≈ 10.5, J(H−C(γ.1), H′−C(δ.1)) = 11.6, 7.2)	3.524
H″−C(δ.1)	3.513	3.477 (J(H″−C(δ.1), H″−C(δ.1)) ≈ 10.5, J(H−C(γ.1), H″−C(δ.1)) = 8.5, 1.4)	3.510
H″−C(δ.2)	3.494	3.305	
H′−C(β.3)	3.242 (J(H−C(5.3), H′−C(β.3)) = 0.8, J(H−C(α.3), H′−C(β.3)) = 9.2, J(H″−C(β.3), H−C(β.3)) ≈ 16)	3.220	3.237
H″−C(β.3)	3.080 (J(H−C(α.3), H″−C(β.3)) = 5.0, J(H′−C(β.3), H″−C(β.3)) ≈ 16)	3.220	3.044 (J(H−C(α.3), H″−C(β.3)) = 9.5, J(H′−C(β.3), H″−C(β.3)) = 15.7)
PhCH_2CH$_2$	2.867, 2.844	2.875, 2.875	2.833, 2.833
PhCH$_2$CH_2	2.631, 2.596	2.605, 2.605	2.441 ($J_{gem} = 8.9$, $J_{vic} = ca.$ 7, 15.1), 2.324 ($J_{gem} = 8.7$, $J_{vic} = ca.$ 7, 15.1)
H′−C(β.1)	2.168 ($J = 7.4$, 12.3, 15.4)	2.242	2.195
H′−C(β.2)	2.082	2.344	n. d.
H′−C(γ.1)	1.957	2.038	1.801
H′−C(γ.2)	1.926	1.827	1.786
H″−C(γ.1)	1.878	1.878	1.716
H″−C(β.2)	1.835	2.070	n. d.
H″−C(β.1)	1.815	1.780	1.937
H″−C(γ.2)	1.310	1.437	1.606

Pro, Fmoc-Pro, and 3-phenylpropanoic acid with the deprotected N^{π}-methyl-L-histidine-loaded resin (147 mg), with a double coupling for the last Pro residue. For capping, the resin was shaken with cold CH_2Cl_2/CF_3COOH/H_2O/^{i}Pr$_3$SiH, filtered, and washed with CH_2Cl_2/CF_3COOH (*ca.* 9 : 1, 2 ml). The combined org. phase was added

Table 6. *^{13}C-NMR Data* (125 MHz, CD_3CN/*ca.* 10 µl of CF_3COOH) *and Assignments for the Three Conformers of Tripeptide* **14**. δ(C) in ppm.

	δ(C)				δ(C)		
	14A	**14B**	**14C**		**14A**	**14B**	**14C**
CO(.2)	173.25	172.93	172.98	Me(O.3)	53.39	53.22	n.d.
$PhCH_2CH_2CO$.0	172.70	174.53	173.46	C(α.3)	51.53	51.91	51.51
CO(.1)	172.63	172.25	n.d.	C(δ.1)	48.48	48.82	48.06
CO(.3)	171.44	171.32	171.50	C(δ.2)	48.23	44.98	n.d.
C_{ipso}	142.38	141.97	142.24	$PhCH_2CH_2$	36.50	35.84	36.79
C(2.3)	136.00	136.07	135.99	Me(N^{π}.3)	34.54	34.38	n.d.
C(4.3)	132.15	132.80	132.15	$PhCH_2CH_2$	31.33	31.48	31.87
C_o	129.36	129.85	n.d.	C(β.2)	29.57	31.65	n.d.
C_m	129.33	129.35	n.d.	C(β.1)	29.47	29.59	31.31
C_p	127.05	127.03	127.04	C(β.3)	26.27	25.31	n.d.
C(5.3)	119.06	118.60	n.d.	C(γ.2)	25.74	22.85	25.79
C(α.2)	61.25	61.82	61.27	C(γ.1)	25.47	25.89	23.30
C(α.1)	59.59	59.95	60.16				

dropwise into cold *t*BuOMe (200 ml), kept at $-75°$ for 1 h, and then centrifuged. Additional product was isolated after concentration of the supernatant *t*BuOMe soln. The total yield was 48 mg of crude peptide (4–6% rel. to the determined loading of the resin). The crude product was purified by reversed-phase HPLC (*C18*; gradient: H_2O, 0.001% $CF_3COOH \rightarrow$ MeCN, 0.001% CF_3COOH): 23 mg of >95% pure (by reversed-phase HPLC) **15** as the CF_3COOH adduct (2–3% yield rel. to the determined loading). NMR: slowly exchanging conformers **15A** (72%), **15B** (23%), and **15C** (5%). ^{1}H-NMR (400 MHz, CD_3OD)*[5]: 8.85 (*s*, H–C(2.4), **B**); 8.77 (*s*, H–C(2.4), **A**); 8.73 (*s*, H–C(2.4), **C**); 7.47 (*s*, H–C(5.4), **B**); 7.45 (*s*, H–H–C(5.4), **A**); 7.36–7.15 (*m*, H*p*, **A**–**C**, H–C(5.4), **C**); 4.85–3.8 (*m*, 9 H–C(α), **A**–**C**); 3.92 (*s*, Me(N^{π}.4), **B**); 3.9 (*m*, 3 H–C(α), **A**–**C**); 3.88 (*s*, Me(N^{π}.4), **A**); 3.85 (*s*, Me(N^{π}4), **C**); 3.8–2.7 (*m*, 3 CH_2(β.4), **A**–**C**, 9 CH_2(δ.Pro), **A**–**C**); 3.1–1.6 (*m*, 9 CH_2(β.Pro), **A**–**C**, 9 CH_2(γ.Pro), **A**–**C**). ^{13}C-NMR (100 MHz, CD_3OD)[5]): 175.0 (CO, **B**); 174.3 (CO, **A**); 174.1 (CO, **C**); 173.8 (CO, **B**); 173.5 (CO, **A**); 173.4 (CO, **B**); 173.3 (CO, **A**); 173.0 (CO, **C**); 172.7 (CO, **A**); 172.6 (CO, **C**); 172.5 (CO, **B**); 172.2 (CO, **C**); 142.5 (C(1.0), **C**); 142.4 (2 C(1.0), **A**, **B**); 137.1 (C(2.4), **B**), 136.6 (2 C(2.4), **A**, **C**); 133.1 (C(4.4), **B**); 132.8 (C(4.4), **C**); 132.7 (C(4.4), **A**); 129.7–129.4 (C_o, C_m, **A**–**C**); 127.4 (C_p, **B**); 127.3 (C_p, **A**, **C**); 120.1 (C(3.4), **A**); 119.9 (C(3.4), **C**); 119.1 (C(3.4), **B**); 62.2 (C(α.123), **A**); 62.1 (C(α.Pro), **C**), 61.7 (C(α.Pro), **B**); 60.7 (C(α.Pro), **C**); 60.5 (C(α.Pro), **C**); 60.3 (C(α.Pro), **A**); 59.9 (C(α.Pro), **B**); 59.3 (C(α.Pro), **A**); 59.4 (C(α.Pro), **B**); 52.0 (C(α.4), **C**); 51.7 (C(α.4), **A**); 51.4 (C(α.4), **B**); 48.7–48.1 (3 C(δ.Pro), **A**–**C**); 37.3 ($PhCH_2CH_2$, **A**–**C**); 34.0 (Me(N^{π}.4), **B**); 33.9 (Me(N^{π}.4), **C**); 33.9 (Me(N^{π}.4), **A**); 33.5–23.7 (9 C(β.Pro), **A**–**C**, 9 C(γ.Pro), **A**–**C**), 3 C(β.His), **A**–**C**). HR-MALDI-MS: 593.308 (MH^+, $C_{31}H_{41}N_6O_6^+$; calc. 593.309 for monoisotopic mass).

N^{α}-*(1-Oxo-3-phenylpropyl)*-L-*prolyl*-L-*prolyl*-D-*prolyl*-N^{π}-*methyl*-L-*histidine Methyl Ester* (**16**). A soln. of **15** (17.7 mg, 0.025 mmol) and 4-methylbenzenesulfonic acid (17.3 mg, 0.10 mmol) in abs. MeOH (5.0 ml) was refluxed for 2 h and stirred for additional 16 h at 25°. After evaporation, the residue was dissolved in 0.5M aq. $NaHCO_3$ (1 ml) and extracted with AcOEt (7 × 1 ml), the org. phase dried ($MgSO_4$) and evaporated, and the residue dried under h.v. (6.9 mg, 45%). The aq. solution was adsorbed on a *C18* cartridge (preconditioned with 0.5M aq. $NaHCO_3$). The *C18* cartridge was washed neutral with H_2O, and an additional amount of crude product (4.1 mg, 27%) was eluted with MeOH. Both fractions were of equal purity (>90% by anal. reversed-phase HPLC) and were combined for the NMR experiments. NMR: conformers **16A** (90%) and **16B** (10%) in slow exchange. ^{1}H- and ^{13}C-NMR: *Tables 7* and *8*. HR-MALDI-MS: 607.324 (MH^+, $C_{32}H_{43}N_6O_6^+$, calc. 607.324 for monoisotopic mass).

3. *Simulations. Hardware:* Octane (*SGI*). *Software:* Molecular modeling: InsightII, version 98.0 (CDiscover 3 module of InsightII und standalone CDiscover (BTCL)) [42]; NMR processing: XWinnmr, v. 2.6

---

[5]) The boldface capital letters refer to the respective conformer. Signal designations H–C(α.Pro) indicate that the type but not the position of the residue could be assigned.

Table 7. *^{1}H-NMR Data* (500 MHz, CD_3CN/*ca.* 10 µl of CF_3COOH) *and Assignments for the Two Conformers of Tetrapeptide* **16**. δ(H) in ppm, J in Hz.

	δ(H)	
	16A	**16B**
H–C(2.4)	8.369	8.363
H–N(α.4)	7.746 (J(H–C(α.4), H–N(α.4)) = 8.5)	7.736 (J(H–C(α.4), H–N(α.4)) = 8.2)
H–C(5.4)	7.339	7.309
2 H_m	7.290	n.d.
2 H_o	7.235	7.210
H_p	7.210	7.282
H–C(α.1)	4.636 (J(H–C(β.1), H–C(α.1)) = 5.4, 8.5)	4.262
H–C(α.4)	4.613 (J(H′–C(β.4), H–C(α.4)) = 4.5, J(H″–C(β.4), H–C(α.4) = 10.0, J(H–N(α.4), H–C(α.4)) = 8.5)	4.549 J(H–C(β.4), H–C(α.4)) = 7.5, 7.5)
H–C(α.2)	4.550 (J(H–C(β.2), H–C(α.2)) = 7.4, 7.4)	4.511 (J(H–C(β.2), H–C(α.2)) = 4.3, 8.6)
H–C(α.3)	4.431 (J(H–C(β.1), H–C(α.3)) = 3.2, 8.0)	4.780
H′–C(δ.2)	3.851	3.513
H′–C(δ.3)	3.815	n.d.
Me(N^{π}.4)	3.776	3.755
Me(O.4)	3.661	3.727
H″–C(δ.3)	3.552	n.d.
H″–C(δ.2)	3.546	3.297
H′–C(δ.1)	3.515	3.687
H″–C(δ.1)	3.444	3.466
H′–C(β.4)	3.271 (J(H–C(5.4), H′–C(β.4)) = 0.5, J(H–C(α.4), H′–C(β.4)) = 4.6, J(H″–C(β.4), H′–(β.4)) = 15.5)	3.252
H″–C(β.4)	2.974 (J(H–C(α.4), H″–(β.4)) = 9.9, J(H′–C(β.4), H″–(β.4)) = 15.6)	2.961
PhCH_2CH_2	2.879	2.833
PhCH_2CH_2	2.661	2.453
H′–C(β.2)	2.264	2.291
H′–C(β.1)	2.211	2.271
H′–C(γ.2)	2.108	1.750
H′–C(γ.3)	2.052	1.745
H′–C(β.3)	2.042	2.287
H″–C(γ.2)	1.993	1.642
H″–C(γ.3)	1.867	1.647
H″–C(β.2)	1.852	1.940
H′–C(γ.1)	1.830	1.955
H″–C(γ.1)	1.816	1.576
H″–C(β.1)	1.764	n.d.
H″–C(β.3)	1.298	1.929

(*Bruker*); signal assignment of 2D-NMR spectra: SPARKY, v. 3.106 with Python extensions [40]; structure calculation: DYANA, v. 1.5 [36]; visualization of calculated structures: MOLMOL, v. 2K2 [43] and POVray v. 3.5 [44].

Initial Molecular Modeling. Gas-phase molecular-mechanics calculations were performed with the ESFF forcefield [42][45][46], which has been applied successfully to other macrocyclic Ni-complexes [47]. The starting structures for the simulation of pyridinalkanamine ligands **3**–**9** bound to the side chain at C(13) of F 430 as amides were generated by setting all torsional angles of the ligand to 180° (including the amide bond; '*all-trans*' starting structure). In a typical high-temperature dynamics calculation (HTD; T 1000 K, t 500 ps), the atoms of the side chain at C(13) of F 430 were fixed according to the X-ray structure of the enzyme. In a second

Table 8. *^{13}C-NMR Data* (125 MHz, CD_3CN/*ca.* 10 µl of CF_3COOH) *and Assignments for the Three Conformers of Tetrapeptide* **16**. δ(C) in ppm.

	δ(C)			δ(C)	
	16A	**16B**		**16A**	**16B**
$PhCH_2CHCO$	173.36	174.54	MeO	53.39	53.46
CO(.3)	173.14	172.61	C(α.4)	51.64	51.98
CO(.2)	172.92	n.d.	C(δ.1)	48.85	48.57
CO(.1)	172.06	172.94	C(δ.2)	48.65	48.30
CO(.4)	171.26	171.45	C(δ.3)	48.34	48.35
C_{ipso}	142.05	142.05	$PhCH_2CH_2$	36.86	36.69
C(2.4)	135.98	135.87	Me(N^{π}.4)	34.50	34.47
C(4.4)	132.20	132.26	$PhCH_2CH_2$	31.60	32.15
C_m	129.49	n.d.	C(β.3)	30.11	30.79
C_o	129.45	129.41	C(β.1)	29.20	28.78
C_p	127.29	127.24	C(β.2)	28.99	30.82
C(5.4)	119.55	119.40	C(γ.2)	26.19	23.52
C(α.3)	61.40	n.d.	C(β.4)	25.89	n.d.
C(α.2)	59.971	60.60	C(γ.1)	25.53	26.36
C(α.1)	59.65	60.48	C(γ.3)	24.76	n.d.

run of HTD with ligands **3**–**9**, starting structures with manually adjusted dihedral angles to give a U-shaped spacer–ligand conformation were used ('random structure'). The archive files containing the calculated minimized structures were merged and analyzed together (2000 frames).

To generate the starting structure of bound peptidic spacers like **10** or **11**, the ligands were first pre-minimized (cvff forcefield) as isolated peptides to generate a U-shaped loop consistent with the geometric requirements and were then attached to the corresponding F 430 monoacid for the HTD run. Histidine was methylated at the N^{π}-position to avoid possible complications arising from tautomeric forms of the imidazole moiety. The ω backbone angles of the peptidic spacer–ligands including the amide bond to the side chain of F 430 were fixed at 180°.

As an alternative to HTD, a second series of calculations used starting structures obtained by a systematic variation of the torsional angles of all freely rotating single bonds in steps of 60 degrees, which were then minimized by molecular mechanics (MM) without any additional restraints. The relevant distances, angles, and dihedral angles were extracted from the resulting coordinates with a BTCL script, and its output was analyzed by a *Perl* script, which eliminated identical conformers and sorted the remaining structures according to the total energy and their ability to coordinate. Relative energies were used to estimate the molar fraction of coordinating structures. *Tables 1* and *2* summarize the HTD and MM results by listing the data for the calculated conformer with the lowest energy overall and the conformer with the lowest energy among those that are able to coordinate.

Generation of Distance Restraints. Cross-peak volumes of the ROESY spectra with $t_m = 150$ ms were integrated and normalized according to the molar fraction of the corresponding conformer as determined by integration in the 1D spectra. Cross-peak volumes were converted into distance restraints by using the two-spin approximation and known distances in the rigid imidazole part of the histidine residue for calibration (see Tables *9*–*11*).

Structure Calculation. To use the information on the puckering of the proline rings as additional restraints in the calculations, the standard library of DYANA had to be adapted. The five-membered rings were opened between C(γ) and C(δ) to allow torsional dynamics of the dihedral angles χ_1, χ_2, and χ_4. Ring closure was enforced by a hard distance constraint of 1.5 Å between C(γ) and C(δ).

Refinement of the Molecular Modeling. To refine the results obtained after the HTD and MM simulations of 3^3,8^3,12^2,18^2-tetra-*O*-methyl-13^3-**L**-F 430 (**L** = ligand derived from **10** or **11**), the following averaged values were extracted from the solution structures of **14A**, **14B**, and **16A**: the angles ω, ψ, and ϕ of each amino acid, the backbone angles χ_1, χ_2, and χ_4 in case of L-Pro and D-Pro and χ_1, χ_2, and χ_4 in case of His, all H–H distances < 5 Å (61 restraints in the case of **14A**, 92 restraints in the case of **14B**, and 83 restraints in the case of **16A**), the distance between the carbonyl O-atom of the acyl group and N^{τ} of the His residue, and, if present, H-bond

Table 9. *NOE-Derived Distance Restraints for Conformer* **14A**

NOE	Lower limit [Å]	Upper limit [Å]	NOE	Lower limit [Å]	Upper limit [Å]
$PhCH_2CH_2(H')-C(5.3)$	1.9	2.8	$H-C(2.3)-Me(N^{\pi}.4)$	2.0	3.1
$H-C(\alpha.1)-H''-C(\beta.1)$	2.7	4.1	$PhCH_2CH_2(H')-H-C(\alpha.1)$	3.2	4.9
$H-C(\alpha.1)-H'-C(\beta.1)$	2.0	3.0	$PhCH_2CH_2(H')-H-C(\delta.1)$	1.5	2.2
$H-C(\alpha.1)-H'-C(\gamma.1)$	3.5	5.3	$PhCH_2CH_2(H')-H-C(\alpha.1)$	3.4	5.0
$H-C(\alpha.1)-H''-C(\gamma.1)$	3.3	4.9	$H-C(\alpha.1)-H''-C(\delta.2)$	2.3	3.5
$H-C(\delta.1)-H''-C(\gamma.1)$	2.0	3.0	$H'-C(\beta.1)-H''-C(\delta.2)$	2.2	3.3
$H-C(\alpha.2)-H'-C(\beta.2)$	2.0	3.0	$H''-C(\beta.1)-H''-C(\delta.2)$	2.3	3.5
$H-C(\alpha.2)-H''-C(\beta.2)$	2.2	3.3	$H-C(\alpha.2)-H-N(\alpha.3)$	2.4	3.7
$H-C(\alpha.2)-H''-C(\delta.2)$	2.9	4.4	$H''-C(\beta.2)-H-N(\alpha.3)$	2.8	4.2
$H-C(\alpha.2)-H'-C(\delta.2)$	2.9	4.3	$H'-C(\gamma.2)-H-N(\alpha.3)$	3.3	5.0
$H'-C(\beta.2)-H'-C(\delta.2)$	2.6	3.8	$H''-C(\delta.2)-H-N(\alpha.3)$	3.0	4.5
$H-N(\alpha.3)-H-C(\alpha.3)$	2.5	3.8	$H'-C(\beta.3)-H-C(\alpha.2)$	3.4	5.1
$H-N(\alpha.3)-H'-C(\beta.3)$	2.9	4.3	$H_p-Me(O.3)$	4.5	6.7
$H-N(\alpha.3)-Me(O.3)$	3.1	4.7	$H-C(\alpha.1)-H-N(\alpha.3)$	3.5	5.2

Table 10. *NOE-Derived Distance Restraints for Conformer* **14B**

NOE	Lower limit [Å]	Upper limit [Å]	NOE	Lower limit [Å]	Upper limit [Å]
$H-C(\alpha.1)-H'-C(\beta.1)$	1.6	2.6	$H''-C(\gamma.2)-H''-C(\delta.2)$	1.7	3.0
$H-C(\alpha.1)-H''-C(\beta.1)$	1.8	3.0	$H-C(\alpha.3)-H-C(5.3)$	2.0	3.5
$H-C(\alpha.1)-H'-C(\gamma.1)$	2.5	4.2	$H-C(\alpha.3)-H-N(\alpha.3)$	2.3	4.1
$H-C(\alpha.1)-H''-C(\gamma.1)$	1.9	3.2	$H-C(\beta.3)-H-N(\alpha.3)$	2.2	3.9
$H-C(\alpha.2)-H'-C(\beta.2)$	1.6	2.8	$H-C(5.3)-H-C(2.3)$	2.7	4.6
$H-C(\alpha.2)-H''-C(\beta.2)$	1.4	2.5	$H-C(\alpha.1)-H-C(\alpha.2)$	1.5	2.8
$H-C(\alpha.2)-H'-C(\delta.2)$	2.4	4.1	$H''-C(\beta.1)-H-C(\alpha.2)$	1.6	2.9
$H-C(\alpha.2)-H''-C(\delta.2)$	2.8	4.7	$H-C(\alpha.2)-H-N(\alpha.3)$	2.3	4.1
$H'-C(\beta.2)-H''-C(\gamma.2)$	1.7	2.8	$H''-C(\delta.2)-H-N(\alpha.3)$	2.3	3.9
$H'-C(\gamma.2)-H''-C(\delta.2)$	2.0	3.3	$H-C(\alpha.1)-H-N(\alpha.3)$	1.9	3.3

distances. The torsional angles of **14A**, **14B**, and **16A**, together with the most-significant H–H distances, the C=O ··· N^{τ}-distance and H-bond distances of the corresponding conformer were used as permanent restraints in a refined HTD simulation of $3^3,8^3,12^2,18^2$-tetra-*O*-methyl-13^3-**L**-F 430 (**L** = ligand derived from **10** or **11**) and $8^3,12^2,13^2,18^2$-tetra-*O*-methyl-3^3-**L**-F 430 (**L** = ligand derived from **10** or **11**). Simulations were run for *T* 298, 400, 700, and 1000 K to test the influence of the temp. on the number of calculated conformers. In one series of calculations, distances to protons H_o, $PhCH_2CH_2$, and $PhCH_2CH_2$ of the model compounds **14** and **16** were used as restraints between the peptide part and the analogous protons of F 430 (H–C(12), $CH_2(13^1)$, $CH_2(13^2)$ (*A*). In a second series, only the distances within the peptide part and no distance restraints within or to the F 430 part were considered (*B*). The simulations were run under the following conditions: *A*, T = 298 or 400 K; *B*, *T* = 400, 700, or 1000 K. The results of these HTD simulations for **14A** and **14B** are summarized in *Tables 3* and *4*. For **16A**, no frame with a capability to coordinate was found at all.

Table 11. *NOE-Derived Distance Restraints for Conformer* **16A**

NOE	Lower limit [Å]	Upper limit [Å]	NOE	Lower limit [Å]	Upper limit [Å]
H_o–PhCH$_2$CH_2	2.6	4.5	H′–C(β.4)–Me(O.4)	4.0	5.9
H_o–PhCH_2CH$_2$	2.2	3.9	H″–C(β.4)–H–N(α.4)	3.4	5.0
H–C(α.1)–H′–C(β.1)	2.0	3.1	H″–C(β.4)–H–C(2.4)	2.9	4.8
H–C(α.1)–H″–C(β.1)	2.3	4.0	H″–C(β.4)–Me(N^{π}.4)	2.0	3.2
H–C(α.1)–H′–C(γ.1)	2.5	3.9	Me(N^{π}.4)–H–C(5.4)	2.2	3.5
H′–C(β.1)–H″–C(δ.1)	2.2	4.8	PhCH$_2$CH_2–H′–C(δ.1)	2.0	3.0
H–C(α.2)–H′–C(β2)	2.0	3.0	PhCH$_2$CH_2–H″–C(δ.1)	1.7	3.2
H–C(α.2)–H″–C(β.2)	2.3	3.5	H–C(α.1)–H′–C(δ.2)	2.0	3.1
H–C(α.2)–H″–C(γ.2)	2.4	3.9	H–C(α.2)–H′–C(δ.3)	2.1	3.3
H′–C(β.2)–H′–C(δ.2)	2.2	3.8	H–C(α.2)–H–C(2.4)	3.3	5.2
H′–C(γ.2)–H′–C(δ.2)	2.1	3.2	H–C(α.2)–H–N(α.4)	2.9	4.5
H″–C(γ.2)–H′–C(δ.2)	2.1	3.3	H′–C(δ.3)–H–N(α.4)	3.2	6.6
H–C(α.4)–H–C(2.4)	2.9	4.9	H″–C(β.1)–H′–C(β.4)	2.5	4.4
H–C(α.4)–H–N(α.4)	2.7	4.4	H′–C(δ.1)–H′–C(β.4)	2.9	4.6
H–C(α.4)–Me(N^{π}.4)	2.4	3.6	H″–C(δ.1)–H′–C(β.4)	2.9	4.8
H′–C(β.4)–H–C(2.4)	2.8	4.2	H″–C(γ.1)–H′–C(β.4)	2.7	4.2
H′–C(β.4)–H–N(α.4)	2.7	4.5	PhCH_2CH$_2$–Me(O.4)	3.7	5.6
H′–C(β.4)–Me(N^{π}.4)	2.5	3.8			

REFERENCES

[1] W. Grabarse, S. Shima, F. Mahlert, E. C. Duin, R. K. Thauer, U. Ermler, in ' Handbook of Metalloproteins', Eds. A. Messerschmidt, R. Huber, T. Poulos, K. Wieghart, Wiley, Chichester, 2001, p. 897.
[2] R. K. Thauer, *Microbiology* **1998**, *144*, 2377.
[3] J. Ellermann, R. Hedderich, R. Böcher, R. K. Thauer, *Eur. J. Biochem.* **1988**, *172*, 669.
[4] T. A. Bobik, K. D. Olson, K. M. Noll, R. S. Wolfe, *Biochem. Biophys. Res. Commun.* **1987**, *149*, 455.
[5] A. Pfaltz, B. Jaun, A. Fässler, A. Eschenmoser, R. Jaenchen, H. H. Gilles, G. Diekert, R. K. Thauer, *Helv. Chim. Acta* **1982**, *65*, 828.
[6] D. A. Livingston, A. Pfaltz, J. Schreiber, A. Eschenmoser, D. Ankel-Fuchs, J. Moll, R. Jaenchen, R. K. Thauer, *Helv. Chim. Acta* **1984**, *67*, 334.
[7] A. Fässler, A. Kobelt, A. Pfaltz, A. Eschenmoser, C. Bladen, A. R. Battersby, R. K. Thauer, *Helv. Chim. Acta* **1985**, *68*, 2287.
[8] G. Färber, W. Keller, C. Kratky, B. Jaun, A. Pfaltz, C. Spinner, A. Kobelt, A. Eschenmoser, *Helv. Chim. Acta* **1991**, *74*, 697.
[9] U. Ermler, W. Grabarse, S. Shima, M. Goubeaud, R. K. Thauer, *Science (Washington, D.C.)* **1997**, *278*, 1457.
[10] W. Grabarse, F. Mahlert, E. C. Duin, M. Goubeaud, S. Shima, R. K. Thauer, V. Lamzin, U. Ermler, *J. Mol. Biol.* **2001**, *309*, 315.
[11] S. P. J. Albracht, D. Ankel-Fuchs, R. Böcher, J. Ellermann, J. Moll, J. W. v. d. Zwaan, R. K. Thauer, *Biochim. Biophys. Acta* **1988**, *955*, 86.
[12] B. Jaun, A. Pfaltz, *J. Chem. Soc., Chem. Commun.* **1986**, 1327.
[13] C. Holliger, A. J. Pierik, E. J. Reijerse, W. R. Hagen, *J. Am. Chem. Soc.* **1993**, *115*, 5651.
[14] M. Goubeaud, G. Schreiner, R. K. Thauer, *Eur. J. Biochem.* **1997**, *243*, 110.
[15] J. Telser, R. Davydov, Y.-C. Horng, S. W. Ragsdale, B. M. Hoffman, *J. Am. Chem. Soc.* **2001**, *123*, 5853.
[16] J. Telser, Y.-C. Horng, D. F. Becker, B. M. Hoffman, S. W. Ragsdale, *J. Am. Chem. Soc.* **2000**, *122*, 182.
[17] T. Wondimagegn, A. Ghosh, *J. Am. Chem. Soc.* **2001**, *123*, 1543.
[18] A. Berkessel, *Bioorg. Chem.* **1991**, *19*, 101.
[19] B. Jaun, *Helv. Chim. Acta* **1990**, *73*, 2209.
[20] V. Pelmenschikov, M. R. A. Blomberg, P. E. M. Siegbahn, R. H. Crabtree, *J. Am. Chem. Soc.* **2002**, *124*, 4039.
[21] S. Rospert, R. Böcher, S. P. J. Albracht, R. K. Thauer, *FEBS Lett.* **1991**, *291*, 371.

[22] J. Telser, Y.-C. Fann, M. W. Renner, J. Fajer, S. Wang, H. Zhang, R. A. Scott, B. M. Hoffman, *J. Am. Chem. Soc.* **1997**, *119*, 733.
[23] C. L. Hamilton, M. W. Renner, R. A. Scott, *Biochim. Biophys. Acta* **1991**, *1074*, 312.
[24] E. C. Duin, N. J. Cosper, F. Mahlert, R. K. Thauer, R. A. Scott, *J. Biol. Inorg. Chem.* **2003**, *8*, 141.
[25] C. Finazzo, J. Harmer, C. Bauer, B. Jaun, E. C. Duin, F. Mahlert, M. Goenrich, R. K. Thauer, S. Van Doorslaer, A. Schweiger, *J. Am. Chem. Soc.* **2003**, *125*, 4988.
[26] a) C. Bauer, B. Jaun, *Helv. Chim. Acta* **2003**, *86*, 4254; b) R. Geiss, Ph. D. Thesis, ETH-Zürich, Zürich, 1998.
[27] K. Barlos, D. Gatos, J. Kallitsis, G. Papaphotiu, P. Sotiriu, W. Yao, W. Schaefer, *Tetrahedron Lett.* **1989**, *30*, 3947.
[28] K. G. Barlos, D. Gatos, G. Papaphotiou, W. Schaefer, *Liebigs Ann. Chem.* **1993**, 215.
[29] K. Barlos, D. Gatos, S. Kutsogianni, G. Papaphotiou, C. Poulos, T. Tsegenidis, *Int. J. Pept. Protein. Res.* **1991**, *38*, 562.
[30] R. Steinauer, P. White, 'Innovation Perspect. Solid Phase Synth. Collect. Pap., 3rd Int. Symp.', meeting date 1993, Ed. R. Epton, Mayflower, Birmingham, UK, 1994, p. 689.
[31] G. Fischer, *Chem. Soc. Rev.* **2000**, *29*, 119.
[32] C. Grathwohl, K. Wüthrich, *Biopolymers* **1981**, *20*, 2623.
[33] C. Grathwohl, K. Wüthrich, *Biopolymers* **1976**, *15*, 2025.
[34] E. J. Milner-White, L. H. Bell, P. H. Maccallum, *J. Mol. Biol.* **1992**, *228*, 725.
[35] Y. K. Kang, J. S. Jhon, S. J. Han, *J. Pept. Res.* **1999**, *53*, 30.
[36] P. Güntert, C. Mumenthaler, K. Wüthrich, *J. Mol. Biol.* **1997**, *273*, 283.
[37] C. Bauer, Ph. D. Thesis, ETH-Zürich, Zürich, **2003**.
[38] 'Biochemical Nomenclature and Related Documents', 2nd edn., Ed. C. Liébecq, Portland Press, London-Chapel Hill, 1992.
[39] C. Griesinger, R. R. Ernst, *J. Magn. Reson.* **1987**, *75*, 261.
[40] T. D. Goddard, D. G. Kneller, 'SPARKY', v. 3.106, University of California, San Francisco, 2002.
[41] J. Rivier, W. Vale, M. Monahan, N. Ling, R. Burgus, *J. Med. Chem.* **1972**, *15*, 479.
[42] 'Module CDiscover, Program InsightII', v. 98, Accelrys Inc., San Diego, USA.
[43] R. Koradi, M. Billeter, K. Wüthrich, *J. Mol. Graphics* **1996**, *14*, 51.
[44] 'POV-Ray for Mac OS X', v. 3.5 (http://www.povray.org).
[45] S. Barlow, A. L. Rohl, D. O'Hare, *Chem. Commun.* **1996**, 257.
[46] S. Barlow, A. L. Rohl, S. Shi, C. M. Freeman, D. O'Hare, *J. Am. Chem. Soc.* **1996**, *118*, 7578.
[47] N. Jäger, U. Schilde, *Struct. Chem.* **1998**, *9*, 77.

Received September 24, 2003